Developmental Biology 384 (2013) 114–127

Contents lists available at ScienceDirect

Developmental Biology

journal homepage: www.elsevier.com/locate/developmentalbiology

MyoD-expressing progenitors are essential for skeletal myogenesis and satellite cell development

William M. Wood, Shervin Etemad, Masakazu Yamamoto, David J. Goldhamer *

Department of Molecular and Cell Biology, University of Connecticut Stem Cell Institute, University of Connecticut, Storrs, CT, USA

ARTICLE INFO

Article history:
Received 3 August 2013
Received in revised form
6 September 2013
Accepted 7 September 2013
Available online 17 September 2013

Keywords:
MyoD
Myf-5
Skeletal muscle
Myoblasts
Progenitors
Myogenesis
Mouse embryo
Diphtheria toxin
DTA
Lineage ablation
Stem cells
Satellite cells

ABSTRACT

Skeletal myogenesis in the embryo is regulated by the coordinated expression of the MyoD family of muscle regulatory factors (MRFs). MyoD and Myf-5, which are the primary muscle lineage-determining factors, function in a partially redundant manner to establish muscle progenitor cell identity. Previous diphtheria toxin (DTA)-mediated ablation studies showed that MyoD+ progenitors rescue myogenesis in embryos in which Myf-5-expressing cells were targeted for ablation, raising the possibility that the regulative behavior of distinct, MRF-expressing populations explains the functional compensatory activities of these MRFs. Using *MyoD*^{iCre} mice, we show that DTA-mediated ablation of MyoD-expressing cells results in the cessation of myogenesis by embryonic day 12.5 (E12.5), as assayed by myosin heavy chain (MyHC) and Myogenin staining. Importantly, *MyoD*$^{iCre/+}$;*R26*$^{DTA/+}$ embryos exhibited a concomitant loss of Myf-5+ progenitors, indicating that the vast majority of Myf-5+ progenitors express MyoD, a conclusion consistent with immunofluorescence analysis of Myf-5 protein expression in *MyoD*^{iCre} lineage-labeled embryos. Surprisingly, staining for the paired box transcription factor, Pax7, which functions genetically upstream of MyoD in the trunk and is a marker for fetal myoblasts and satellite cell progenitors, was also lost by E12.5. Specific ablation of differentiating skeletal muscle in ACTA1Cre;*R26*$^{DTA/+}$ embryos resulted in comparatively minor effects on MyoD+, Myf-5+ and Pax7+ progenitors, indicating that cell non-autonomous effects are unlikely to explain the rapid loss of myogenic progenitors in *MyoD*$^{iCre/+}$;*R26*$^{DTA/+}$ embryos. We conclude that the vast majority of myogenic cells transit through a MyoD+ state, and that MyoD+ progenitors are essential for myogenesis and stem cell development.

Introduction

The MyoD family of basic helix-loop-helix muscle transcription factors (MyoD, Myf-5, Myogenin, Mrf4) serves central functions in the regulatory circuitry that controls skeletal muscle determination and differentiation. MyoD and Myf-5 play fundamental roles in muscle lineage determination, and mice lacking both MRF undergo only limited embryonic myogenesis, which is directed by Mrf4 (Kassar-Duchossoy et al., 2004, 2005). Ultimately, embryos lacking both MyoD and Myf-5 are essentially devoid of skeletal muscle and die perinatally (Rudnicki et al., 1993; Kaul et al., 2000; Kassar-Duchossoy et al., 2004, 2005). Loss of either Myf-5 or MyoD, however, result in only minor and transient muscle deficiencies in epaxial and hypaxial myogenesis, respectively (Braun et al., 1992; Rudnicki et al., 1992; Kablar et al., 1997; Tajbakhsh et al., 1997), demonstrating that each MRF can functionally compensate for the other's absence.

Whereas genetic interactions controlling early myogenesis have been intensively investigated, important questions concerning the nature of MyoD and Myf-5 genetic redundancy remain unresolved. For example, it is unclear to what extent the compensatory activities of MyoD and Myf-5 reflect similar molecular activities in myogenic progenitors that express both factors, or arise from regulative behavior of distinct myogenic pools that express either MyoD or Myf-5. Immunostaining and in situ hybridization studies have revealed extensive co-expression, but also considerable cellular heterogeneity, in Myf-5 and MyoD expression, with individual cells or myogenic regions often expressing either MyoD or Myf-5 (Smith et al., 1994; Cossu et al., 1996; Tajbakhsh et al., 1998; Relaix et al., 2005; Gensch et al., 2008; Haldar et al., 2008). Initially, this heterogeneity reflects distinct temporal and spatial patterns of activation of these muscle regulatory genes in early myogenesis, principally in epaxial and hypaxial somite domains (Sassoon et al., 1989; Ott et al., 1991; Smith et al., 1994; Goldhamer et al., 1995; Cossu et al., 1996; Relaix et al., 2005). However, even in the limb buds, where Myf-5 and

* Correspondence to: G24 Biology-Physics Building, 91 N. Eagleville Road, Unit 3125, Storrs, CT 06269, USA.
E-mail address: david.goldhamer@uconn.edu (D.J. Goldhamer).

0012-1606/$ - see front matter © 2013 Elsevier Inc. All rights reserved.
http://dx.doi.org/10.1016/j.ydbio.2013.09.012

MyoD activation is temporally coincident, and at later stages in muscle forming regions that show temporally distinct patterns of activation, myoblasts singly positive for either MyoD or Myf-5 are prevalent (Gensch et al., 2008; Haldar et al., 2008). These data are consistent with the intriguing possibility that developing muscle beds include distinct muscle progenitor populations that could provide the cellular substrates for the engagement of compensatory mechanisms to drive myogenesis when one or more myogenic populations is lost, or when a progenitor population is rendered incapable of myogenic activity due to the loss of either MyoD or Myf-5. However, most studies of MRF expression heterogeneity have utilized immunohistological methods, which provide a static view of MRF expression at discrete stages of development and cannot be used to ascertain the extent to which myoblasts singly positive for MyoD or Myf-5 represent distinct, independent progenitor pools that express only one factor throughout their developmental history. In addition, MyoD and Myf-5 expression are cell cycle regulated (Kitzmann et al., 1998) and have short (<1 h) protein and mRNA half-lives (Thayer et al., 1989; Carnac et al., 1998), which likely contributes to the apparent degree of non-overlap of MyoD and Myf-5 expression.

Cell-specific ablation using Cre-dependent DTA expression provides a powerful means of interrogating progenitor cell dynamics. Results of previous DTA ablation studies suggested the existence of a functionally significant pool of MyoD+ progenitors that do not express Myf-5 (Gensch et al., 2008; Haldar et al., 2008). Thus, ablation of Myf-5-expressing cells had only transient effects on myogenesis; myogenic activity—driven by MyoD+ progenitors—was restored by approximately early fetal stages, generating muscle that appeared normal by histological and ultrastructural criteria. These data are consistent with the existence of at least two distinct myogenic progenitor populations based on the presence or absence of Myf-5 expression and demonstrate the marked regulative capacity of developing skeletal muscle.

We sought to further clarify the interrelationship between embryonic myogenic populations by immunofluorescence analyses, lineage tracing, and targeted DTA-mediated ablation of MyoD-expressing cells using *MyoD*^{iCre} mice (Kanisicak et al., 2009; Yamamoto et al., 2009). The *MyoD*^{iCre} allele allows highly efficient labeling of embryonic and fetal myoblasts, as well as satellite cell progenitors, and is not expressed outside of myogenic populations in the embryo (Kanisicak et al., 2009; Yamamoto et al., 2009). Consistent with previous findings, we observed considerable heterogeneity in MyoD and Myf-5 protein expression at each developmental stage examined. Ablation of MyoD-expressing cells, however, resulted in the loss of myofibers and myogenic progenitors (defined by Pax7 or Myf-5 expression) by E12.5, approximately 2 days after the onset of detectable *MyoD*^{iCre}-dependent reporter gene expression. Disruption of the muscle environment by targeting DTA expression specifically to differentiating muscle cells had a comparatively minor effect on myogenic progenitors, indicating that cell non-autonomous effects cannot explain the rapid loss of Pax7+ or Myf-5+ progenitors following ablation of MyoD-expressing cells. These data show that the vast majority of myogenic progenitors transit through a MyoD+ stage and that myogenesis cannot be rescued by MyoD-non-expressing embryonic progenitors.

Materials and methods

Mice and genotyping

Animal procedures were reviewed and approved by the University of Connecticut's Institutional Animal Care and Use Committee. Production and characterization of *MyoD*^{iCre}, *R26*^{NZG}, and *R26*^{NG} mice was described previously (Kanisicak et al., 2009; Yamamoto et al., 2009). ROSA26-eGFP-DTA (*R26*^{DTA}; Ivanova et al., 2005; JAX #006331), ROSA-DTA (R-DTA; Haldar et al., 2008; Wu et al., 2006; JAX #009669) and ACTA1Cre (Miniou et al., 1999; JAX #006139) mice were purchased from Jackson Laboratories. Experimental animals were on an enriched FVB background. PCR-based genotyping of DNA isolated from tail biopsies or yolk sacs was done as previously described (Miniou et al., 1999; Ivanova et al., 2005; Kanisicak et al., 2009; Yamamoto et al., 2009), except that sucrose was added to a final concentration of 12% for all PCR reactions.

Mouse crosses

To generate experimental embryos for DTA ablation and lineage tracing, the *MyoD*^{iCre} knockin allele and ACTA1Cre transgene were introduced through the male germline to avoid the possibility of premature Cre-mediated recombination due to leaky Cre expression and accumulation in the egg (see Chen et al., 2005 and references therein). As an additional precaution, Cre drivers and DTA or reporter alleles were introduced through different parents, when possible. Typically, heterozygous parents were used for crosses to generate all classes of littermate controls, although in some cases, *R26*$^{DTA/DTA}$ females were used to increase the efficiency of generating experimental embryos. Control embryos were either wild-type, or carried one copy of the Cre driver or DTA allele. No phenotypic differences among these genotypes were observed. Embryos were collected between embryonic day 10.5 (E10.5) and E16.5, with noon on the day of the vaginal plug considered E0.5. Staging of somite-stage embryos was confirmed by morphological criteria (Kaufman, 1992). Except where noted, at least three embryos of each genotype for each developmental stage were examined and representative images are shown.

Histology and immunofluorescence

Embryos derived from crosses that included the Cre-dependent GFP reporter allele, *R26*^{NG}, were immediately fixed in 2% paraformaldehyde (PFA) in PBS (20 mM sodium phosphate, 0.10 M NaCl, pH 7.4) for 2 h at 4 °C, immersed in 15% sucrose in PBS at 4 °C for 2 h, and 30% sucrose O/N before being immersed in OCT compound (Sakura Finetek) and frozen in liquid nitrogen. Embryos from all other crosses were immersed in OCT compound immediately after collection and frozen in liquid nitrogen. Embryos were stored at −80 °C.

Frozen embryos were cryostat sectioned at 12–14 μm, collected on Superfrost Plus slides (Fisher), briefly dried with a hair dryer, and stored at −80 °C. Antigen retrieval was used for detection of all proteins except Myf-5. After thawing, sections derived from fixed embryos were directly processed for antigen retrieval whereas sections from unfixed embryos were first fixed in 2% PFA/PBS for 20 min at 4 °C. For antigen retrieval, slides were washed three times for 5 min each in PBS, incubated for 6 min in −20 °C methanol, and washed as above. Slides were then placed in 10 mM sodium citrate buffer, pH 6.0, and incubated in a 1200 W microwave at 10% power for 20 min, followed immediately with incubation at 4 °C for 20 min.

The following antibodies and working dilutions were used for immunofluorescence. MyoD: monoclonal antibody (mAb) 5.8A (1:50 dilution; catalog # 554130, BD Pharmingen); Myf-5: rabbit polyclonal antiserum (1:200 dilution; catalog # sc-302, Santa Cruz Biotechnology); Myogenin: mAb F5D (1:1 dilution of hybridoma supernatant; Developmental Studies Hybridoma Bank); Pax7: mAb Pax7 (1:1 dilution of hybridoma supernatant; Developmental Studies Hybridoma Bank); Pax3: mAb Pax3 (1:1 dilution of hybridoma supernatant; Developmental Studies Hybridoma Bank); MyHC: mAb MF20 (1:1 dilution of hybridoma supernatant; Developmental Studies

Hybridoma Bank); GFP: chicken polyclonal antiserum (1:250 dilution; catalog # 13970, Abcam).

For detection of MyHC and Myogenin, sections were blocked in M.O.M. blocking solution (Vector Laboratories) O/N at 4 °C, washed two times in PBS for 10 min each, incubated for 30 min in M.O.M. diluent at room temperature (RT), and incubated in primary antibody suspended in M.O.M. diluent for 2 h at RT. After three 5 min washes in PBS, sections were incubated in a 1:250 dilution of M.O.M. Biotinylated Anti-Mouse IgG Reagent (Vector Laboratories) in M.O.M. diluent for 30 min at RT, washed three times for 5 min each in PBS, and incubated for 30 min in 1:400 dilution of Alexa Fluor 555-conjugated Streptavidin (Invitrogen) in M.O.M. diluent for 30 min. After three 5 min washes in PBS, sections were counterstained with DAPI (0.1 μg/ml) and slides coverslipped using Fluoro-Gel (Electron Microscopy Sciences). Immunofluorescence detection of MyoD followed a similar procedure through the primary antibody incubation step. After three 5 min washes in PBS, sections were incubated in a 1:250 dilution of goat anti-mouse Alexa Fluor 568 in PBSMBT (1X PBS, 1.5% Non-fat dried milk, 1.5% BSA, 0.1% Triton X-100) for 1 h at RT, washed as above, and the signal amplified by incubation for 1 h at RT in a 1:250 dilution of donkey anti-goat Alexa Fluor 568 in PBSMBT. Slides were washed, stained with DAPI and coverslipped as above. For Pax7 and Pax3 immunofluorescence, sections were incubated in M.O.M. blocking solution for 2 h at RT, incubated O/N at 4 °C in primary antibody suspended in PBSMBT, washed three times for 5 min each in PBS, and subsequently processed as for MyoD above. For detection of Myf-5, sections were blocked in PBSMBT O/N at 4 °C, incubated for 30 min at RT in primary antibody diluted in PBSMBT, and processed as for MyoD, Pax7 and Pax3 except that goat anti-rabbit Alexa Fluor 568 was used for the secondary antibody. For immunofluorescence detection of GFP, sections were blocked O/N at 4 °C in PBSMBT, washed three times for 5 min each in PBS, incubated in primary antibody diluted in PBSMBT for 1 h at RT, washed in PBS as above, incubated in goat anti-chicken Alexa Fluor 488 diluted in PBSMBT for 1 h at RT, and washed, stained with DAPI and coverslipped as above.

Simultaneous detection of MyoD/GFP and MyoD/Myf-5 followed the MyoD protocol in terms of antigen retrieval, blocking buffer, diluent buffer, incubation times and antibody concentrations. For detection of MyoD and GFP, sections were incubated with both primary antibodies simultaneously and washed in PBS as above. MyoD was then detected by sequential incubation in the secondary (goat anti-mouse Alexa Fluor 568) and tertiary (donkey anti-goat Alexa Fluor 568) antibodies as above. After three 5 min PBS washes, sections were incubated with goat anti-chicken Alexa Fluor 488 to detect GFP (native GFP fluorescence was destroyed by antigen retrieval). Control experiments verified negligible interaction between the bound tertiary antibody and the goat anti-chicken secondary antibody. For detection of MyoD and Myf-5, sections were incubated with both primary antibodies simultaneously, washed in PBS, incubated with both secondary antibodies simultaneously (chicken anti-mouse Alexa Fluor 488 to detect MyoD and goat anti-rabbit Alexa Fluor 568 to detect Myf-5) and washed in PBS. Sections were then sequentially incubated in the tertiary antibodies, donkey anti-goat Alexa Fluor 568 and goat anti-chicken Alexa Fluor 488, with three 5 min PBS washes between antibody incubations. Slides were washed, stained with DAPI and coverslipped as above.

For simultaneous detection of MyoD, Myf-5 and GFP, native GFP fluorescence was photographed prior to antigen retrieval, coverslips were removed, and sections were processed for antigen retrieval and MyoD and Myf-5 immunodetection as above.

Whole mount in situ hybridization and X-gal staining

Whole mount in situ hybridization with digoxigenin-labeled probes was performed as previously described (Henrique et al., 1995; Yamamoto et al., 2007), with minor modifications related to color development and storage. Briefly, for color development, embryos were incubated in BM Purple (Roche Applied Science) overnight at room temperature. After color development, embryos were washed three times in MABT for 3 h, and stored overnight in MABT at room temperature. Embryos were subsequently transferred to 70% ethanol for 30 min at room temperature, rinsed in MABT and stored at 4 °C in MABT. The MyoD probe has been previously described (Yamamoto et al., 2007). The Myf-5 probe represents a 613 nucleotide fragment of the Myf-5 cDNA that was amplified by PCR using the following primers: Forward: 5′-CATATGGACATGACGGACGGC-3′, Reverse: 5′-AGCTGGACACGGAGCTTTTA-3′.

Whole mount X-gal staining for detection of β-galactosidase (β-gal) activity was done as previously described (Yamamoto et al., 2007).

Microscopy and image collection

Imaging of whole mount embryos was performed on a Leica MZFLIII fluorescence stereomicroscope equipped with a Spot RT3 camera and Spot Advanced image capture software (Diagnostic Instruments). Slides were imaged using either a Nikon E600 upright microscope equipped with a Spot RT3 camera or a Nikon A1R four-laser spectral confocal microscope equipped with both a multiline Argon laser (525/50 nm excitation) for Alexa Fluor 488 and a Coherent Sapphire 561 laser (600/50 nm excitation) for Alexa Fluor 568. Separate channels were captured independently and acquired with Nikon NIS-Elements software. All images were processed and assembled in Photoshop with only minor adjustments made to image brightness and contrast, when necessary. Exposure times and post-capture manipulations were identical for comparison groups (e.g. sections from control and DTA embryos at a particular stage). Images that are composites of multiple micrographs are noted in the figure legends.

Results

Cellular heterogeneity in MyoD and Myf-5 protein expression

We first assessed the degree of overlap of MyoD-expressing and Myf-5-expressing cells by immunofluorescence to serve as a baseline for DTA ablation and lineage tracing analyses. We focused on E11.5 and E12.5 embryos, since in Myf-5 lineage-ablated embryos, these stages encompassed the major period of recovery of myogenic activity after an initial loss of MyoD+ progenitors, as revealed by RT-PCR and in situ hybridization analysis for MyoD mRNA (Gensch et al., 2008). Consistent with previous data (Smith et al., 1994; Cossu et al., 1996; Tajbakhsh et al., 1998; Relaix et al., 2005; Gensch et al., 2008; Haldar et al., 2008), we observed substantial cellular heterogeneity in Myf-5 and MyoD expression (Fig. 1). In the myotomes at E11.5, for example, cells positive either for MyoD or Myf-5, as well as double positive progenitors, were readily detected, with single positive progenitors representing the majority of myogenic cells (Fig. 1A, C–E). All three combinations of MRF expression were observed throughout the dorsomedial to ventrolateral extent of the myotomes, although MyoD-expressing cells tended to be less abundant in central myotomes of interlimb somites (data not shown), consistent with the distribution of MyoD mRNA and MyoD-dependent reporter gene activity at this stage (Goldhamer et al., 1992; Faerman et al., 1995; Goldhamer et al., 1995; Chen et al., 2002). All three classes of MRF-expressing progenitors were also present in the premuscle masses of E11.5 forelimb buds, with myoblasts singly positive for Myf-5 being the most prevalent class at this stage (Fig. 1A, H–J; data not shown). A high degree of cellular

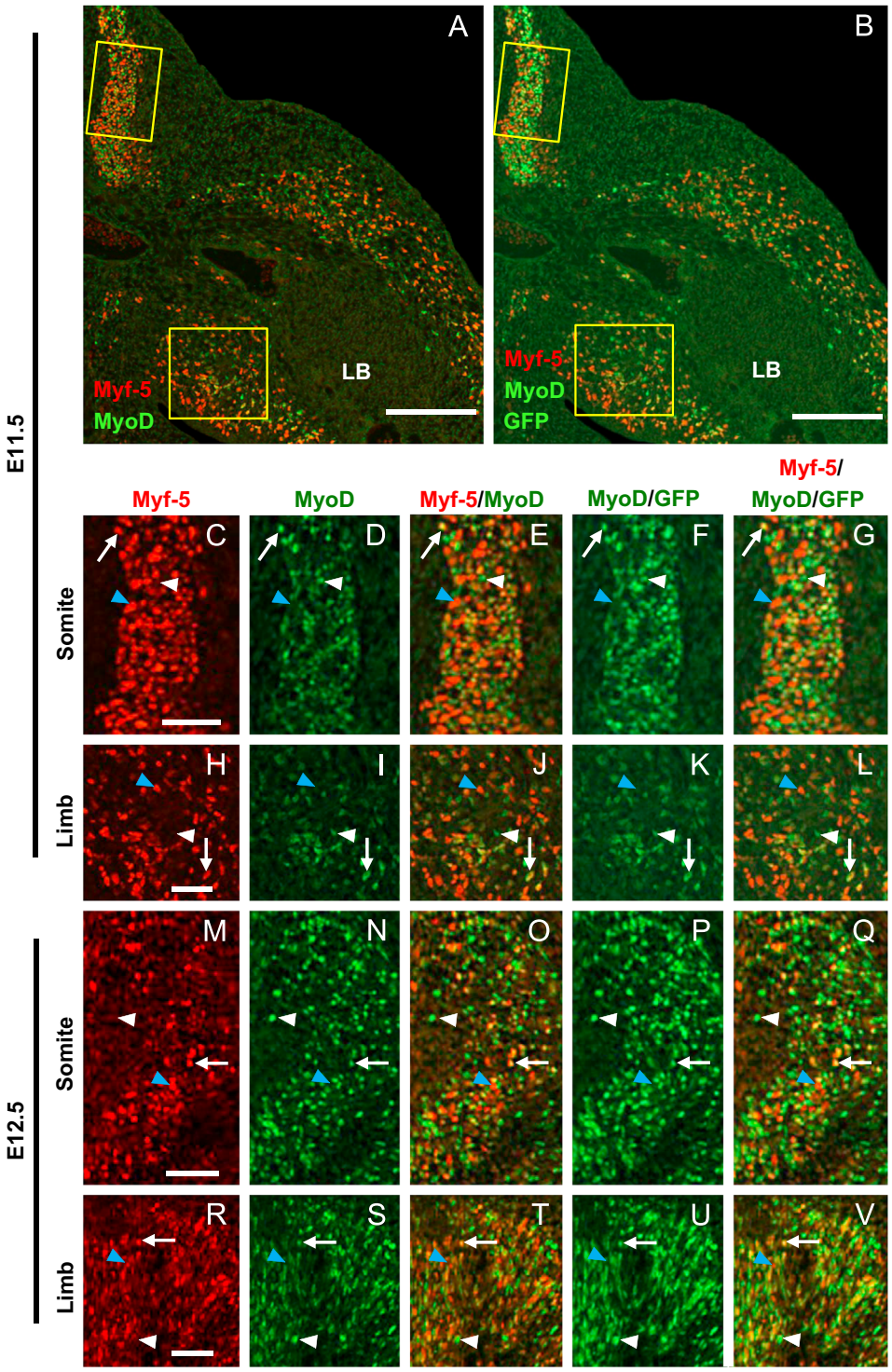

Fig. 1. Cellular heterogeneity in MyoD and Myf-5 protein expression. (A, B) Transverse cryostat section of an E11.5 *MyoD*$^{iCre/+}$;*R26*$^{NG/+}$ embryo stained by immunofluorescence for MyoD and Myf-5 expression. Panel A is a merged double immunofluorescence image; the GFP signal from the Cre-dependent GFP reporter, *R26*^{NG}, was destroyed during antigen retrieval prior to immunofluorescence processing. Panel B was imaged for GFP expression (reflecting activity of the *MyoD*^{iCre} allele) prior to antigen retrieval and subsequently merge with the immunofluorescence image. (C–G) The boxed myotomal region in A and B is shown at higher magnification as single channel and merged images to show heterogeneity in MyoD and Myf-5 expression. (H–L) The boxed forelimb bud region in A and B is shown at higher magnification as single channel and merged images. (M–V) Single channel and merged immunofluorescence images from a forelimb-level myotome or premuscle mass of the proximal forelimb bud of an E12.5 *MyoD*$^{iCre/+}$;*R26*$^{NG/+}$ embryo. Sections were imaged for MyoD and Myf-5 protein expression with or without the GFP lineage marker, as above. Panels A and B are assembled composites of multiple images. Examples of cells positive for both MyoD and Myf-5 (arrows), and singly positive for either MyoD (white arrowheads) or Myf-5 (blue arrowheads) are shown. LB, limb bud. Scale bars represent 200μm in A and B, and 50 μm in C–V.

heterogeneity in MRF expression was also observed at E12.5 (Fig. 1M–O, R–T). Cell counts of MRF+ cells in the ventro-proximal forelimb revealed that myogenic progenitors singly positive for either MyoD (54%) or Myf-5 (31%) were more abundant than cells expressing both MRFs (15%) (n=1878 cells, 5 embryos). Similar results were obtained among progenitors derived from the epaxial myotome (MyoD+Myf-5–, 53%; MyoD–Myf-5+, 29%; MyoD+Myf-5+, 18%) (n=2922 cells, 5 embryos). Although this

enumeration of MRF+ cells should be considered an approximation because of inherent difficulty in identifying progenitors expressing low levels of MyoD or Myf-5, these data reveal substantial heterogeneity among myoblasts populating the developing muscle beds at these developmental stages.

To further address the interrelationships and stability of the myogenic populations described above, we analyzed Myf-5 expression in embryos in which MyoD-expressing cells were stably lineage marked using Cre/loxP recombination methods. For this experiment, we used *MyoD*^{iCre} knockin mice, in which Cre is faithfully and efficiently expressed under endogenous *MyoD* control (Kanisicak et al., 2009; Yamamoto et al., 2009), and a highly sensitive Cre-dependent eGFP reporter, *R26*^{NG} (Yamamoto et al., 2009). First, the dynamics of MyoD protein expression was addressed by comparing MyoD and GFP expression in *MyoD*$^{iCre/+}$;*R26*$^{NG/+}$ embryos. The myotomes and muscle beds of the forelimb buds at E11.5 were highly heterogeneous in terms of MyoD and GFP expression (Fig. S1A–F). This was particularly evident in the forelimb buds, where MyoD+ cells that were negative for the lineage marker (i.e., GFP–) predominated (Fig. S1D–F). By E12.5, however, the number of MyoD+GFP– cells was substantially reduced (Fig. S1G–L), suggesting that the MyoD+GFP– cells at E11.5 represented progenitors that had recently activated *MyoD* expression but had insufficient time to accumulate detectable levels of GFP. Based on published whole mount in situ hybridization analyses (Tajbakhsh et al., 1997; Chen et al., 2002; Chen and Goldhamer, 2004; Kanisicak et al., 2009), the lag between the initiation of *MyoD* expression and accumulation of detectable *MyoD*^{iCre}-dependent reporter gene expression (Figs. 1 and 2; Kanisicak et al., 2009, unpublished observations) was approximately 12–24 h. Given the muscle specificity of *MyoD*^{iCre}-dependent lineage marking (Kanisicak et al., 2009; Yamamoto et al., 2009), MyoD–GFP+ cells observed at E11.5 and E12.5 (Fig. S1) likely represent cells that had expressed *MyoD* at an earlier stage, but not at the time of analysis, consistent with the dynamic nature of MyoD expression.

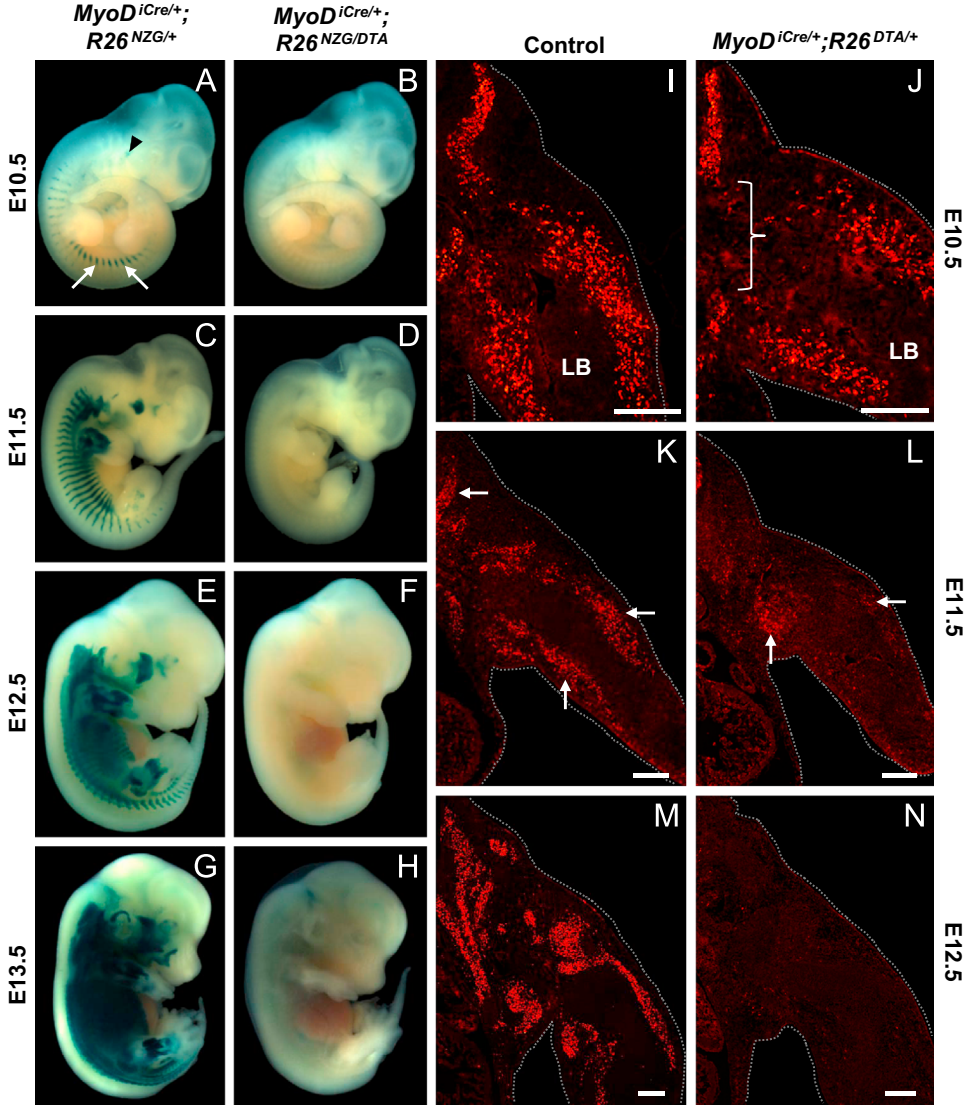

Fig. 2. Efficient translational inhibition/ablation of the MyoD lineage by *MyoD*^{iCre}-directed expression of DTA. (A, C, E, G) *MyoD*^{iCre}-dependent lacZ expression driven by the lacZ reporter, *R26*^{NZG}, was first detected in the myotomes at E10.5 (A), particularly in the hypaxial domains of interlimb somites (arrows), and in progenitors of head musculature (arrowhead). LacZ expression subsequently marked all myogenic areas of the head, trunk and limb buds (C, E, G). (B, D, F, H) LacZ expression was undetectable in embryos carrying the *R26*^{DTA} allele. Slight non-specific "bluing" of larger embryos is common (H). (I–N) MyoD protein expression was lost by E12.5 in *MyoD*$^{iCre/+}$; *R26*$^{DTA/+}$ embryos. At E10.5 (I, J), modest effects of DTA expression were observed in hypaxial myotomes (brackets) and forelimb buds (LB). By E11.5 (K, L), the number of MyoD+ cells and apparent expression levels per cell was greatly reduced. Examples of MyoD+ muscle beds in the control (K), and areas of persistent MyoD expression in a *MyoD*$^{iCre/+}$; *R26*$^{DTA/+}$ embryo, (L) are shown at the arrows. By E12.5 (M, N), MyoD+ cells were essentially undetectable (N). Panels K–N are assembled composites of multiple images. Dotted lines were added to show embryo borders. Scale bars represent 200 μm.

The above analysis shows that the combined use of both lineage marking and immunofluorescence provides a more accurate measure of the size of the MyoD-expressing population than either technique alone. Therefore, we assessed the overlap in Myf-5+ and MyoD+ myoblast populations in *MyoD*$^{iCre/+}$;*R26*$^{NG/+}$ embryos using immunofluorescence for Myf-5, and both lineage marking and immunofluorescence for MyoD. Use of the lineage marker increased the apparent representation of MyoD+ cells at both E11.5 and E12.5. This was most obvious in the myotomes (Fig. 1B–G, M–Q), and probably reflects the earlier activation of MyoD (and therefore the greater contribution of detectable lineage marked cells) relative to the limb buds. Nevertheless, substantial heterogeneity in MyoD and Myf-5 expression was evident in the forelimb buds at E11.5 and in the myotomes at both E11.5 and E12.5 (Fig. 1). The predominance of MyoD+Myf-5– cells in the myotomes at E12.5 probably reflects the down-regulation of Myf-5 expression between E11.5 and E12.5 (Fig. 1C, M), although this analysis cannot rule out the existence of a distinct, Myf-5-non-expressing population. A small number of scattered cells that expressed Myf-5 but not MyoD persisted in the myotomes through E12.5 (Fig. 1P, Q), raising the possibility that a small MyoD-non-expressing population exists. By E12.5, the great majority of myogenic cells of the forelimb buds expressed both proteins (Fig. 1R–V; data not shown).

Efficient DTA-mediated ablation of MyoD-expressing myogenic populations

Cre-dependent DTA ablation strategies were used to test for the existence of a MyoD-negative myoblast population, and to determine if such a population could rescue myogenesis following ablation of MyoD-expressing progenitors. To ablate MyoD-expressing cells, embryos were produced that carry both the *MyoD*^{iCre} allele and the *Rosa26*$^{eGFP\text{-}DTA}$ allele (Ivanova et al., 2005; hereafter referred to as *R26*^{DTA}), allowing for the muscle-specific expression of DTA upon iCre-mediated excision of the floxed stop cassette containing eGFP. To best ensure efficient cell ablation, we used wild-type DTA for most experiments, although an attenuated form of DTA (Wu et al., 2006; Haldar et al., 2008) was used in some cases, where noted, to compare with Myf-5 lineage ablation studies (Haldar et al., 2008).

We first evaluated the effectiveness of DTA-mediated ablation by conducting a developmental time course of *MyoD*^{iCre}-dependent lacZ expression (*R26*^{NZG} allele; Yamamoto et al., 2009) in mice that carry the DTA allele (*MyoD*$^{iCre/+}$;*R26*$^{DTA/NZG}$). At E11.5 through E13.5, control embryos lacking DTA showed robust, muscle-specific β-gal staining (Fig. 2C, E, G) that was essentially identical to the endogenous pattern of *MyoD* expression (Tajbakhsh et al., 1997; Chen et al., 2002; Chen and Goldhamer, 2004; Kanisicak et al., 2009; Yamamoto et al., 2009). E10.5 embryos (Fig. 2A) showed weak β-gal expression, reflecting the aforementioned delay in detectable reporter gene activity relative to endogenous *MyoD* expression. *MyoD*$^{iCre/+}$ embryos carrying *Rosa26*$^{DTA/NZG}$, in contrast, showed no β-gal activity at comparable stages (Fig. 2B, D, F, H), indicating efficient recombination of the *Rosa26*^{DTA} locus among *MyoD*-expressing progenitors of trunk, limb and head musculature. Because both DTA and reporter gene expression were dependent on Cre, these observations do not prove that all myogenic cells that expressed endogenous *MyoD* were targeted for ablation. To address this point, expression of endogenous MyoD protein was assessed in *MyoD*$^{iCre/+}$;*R26*$^{DTA/+}$ embryos. At E10.5, prior to significant Cre-dependent reporter gene expression (Fig. 2A), the number of MyoD+ cells was only modestly reduced in *MyoD*$^{iCre/+}$;*R26*$^{DTA/+}$ embryos relative to control embryos (Fig. 2I, J), particularly in the hypaxial myotomal domains of trunk somites, which represents the region where Cre-dependent reporter gene activity is first detected (Fig. 2A). By E11.5, however, the number of MyoD+ cells and apparent MyoD protein abundance per cell were greatly attenuated (Fig. 2K, L), and by E12.5, MyoD+ cells were rarely observed (Fig. 2M, N). The loss of MyoD immunoreactivity in DTA embryos occurred prior to, or concomitant with, the stage at which *MyoD*^{iCre}-dependent reporter gene expression was initially detected in control embryos (Fig. 2A, C, J, L; Kanisicak et al., 2009; Yamamoto et al., 2009), implying rapid translational inhibition in DTA-expressing cells and rapid turnover of MyoD protein, which has been documented in cultured myoblasts (Thayer et al., 1989; Carnac et al., 1998).

Since DTA is a translational inhibitor, an absence of MyoD immunoreactivity or reporter gene expression does not necessarily reflect the timing of cell ablation. To assess whether MyoD-expressing cells persisted after the loss of MyoD immunoreactivity, and to further document the efficiency of targeting DTA expression to MyoD-expressing cells, we performed whole mount in situ hybridization on DTA and control embryos between E11.5 and E13.5. In contrast to the immunofluorescence data, MyoD transcript levels in E11.5 *MyoD*$^{iCre/+}$;*R26*$^{DTA/+}$ embryos were comparable to controls, except for a small reduction in the forelimb buds (Fig. 3A, D), indicating the persistence of MyoD-expressing cells at a stage when DTA-mediated inhibition of MyoD translation was nearly complete. By E12.5, however, MyoD transcripts were dramatically reduced, being restricted primarily to the dorsal- and ventral-most interlimb body wall muscles, the hindlimb buds, and the myotomes of the tail, the developmentally youngest myotomes of the embryo (Fig. 3B, E) in which activation of DTA expression would have been delayed relative to other myogenic areas. By E13.5, MyoD transcripts were only detected in the most posterior somites in the tail and the hindlimbs, where the signal was barely detectable (Fig. 3C, F). Collectively, these data demonstrate that the *MyoD*^{iCre} allele effectively targets essentially all MyoD-expressing cells for DTA-dependent translational inhibition, and ultimately, ablation (see below).

DTA-mediated ablation of MyoD+ progenitors abolishes myogenesis

Muscle differentiation was assessed in *MyoD*$^{iCre/+}$;*R26*$^{DTA/+}$ embryos by immunofluorescence for the differentiation markers, Myogenin (Fig. S2) and MyHC (Fig. 4). A deficiency in hypaxial myotomal differentiation was already evident at E10.5 in forelimb-level and interlimb somites (Fig. 4A, B), the initial sites of *MyoD*^{iCre} expression in the body (see Fig. 2A). Early epaxial myotomal myogenesis is dependent on Myf-5 (Braun et al., 1992; Kablar et al., 1997; Tajbakhsh et al., 1997) and Mrf4 (Kassar-Duchossoy et al., 2004), prior to the initiation of *MyoD* expression and, accordingly, was not appreciably affected at this stage. In control embryos at E11.5, MyHC staining in the body was primarily observed in myotome-derived muscles and the shoulder region (Fig. 4C). E11.5 represents the earliest stage of detectable muscle differentiation in the forelimbs, and MyHC staining among control embryos varied from barely detectable (data not shown) to the level shown in Fig. 4C. This variation likely reflects small differences in developmental stage among embryos classified as E11.5. In *MyoD*$^{iCre/+}$;*R26*$^{DTA/+}$ embryos, MyHC staining in developing skeletal muscles of the head, trunk and limbs was essentially absent, except for rare cells weakly positive for MyHC in the central myotome (Fig. 4D; data not shown). As expected, cardiac muscle was unaffected in these embryos and stained intensively with mAb MF20, which recognizes all forms of sarcomeric MyHC (Bader et al., 1982). Differentiating skeletal muscle was undetectable in *MyoD*$^{iCre/+}$*R26*$^{DTA/+}$ embryos at E12.5, except for rare individual cells in the limb or trunk (Fig. 4F, data not shown). This is in striking contrast to control embryos, in which MyHC expression is pronounced in all muscle forming areas of the trunk and

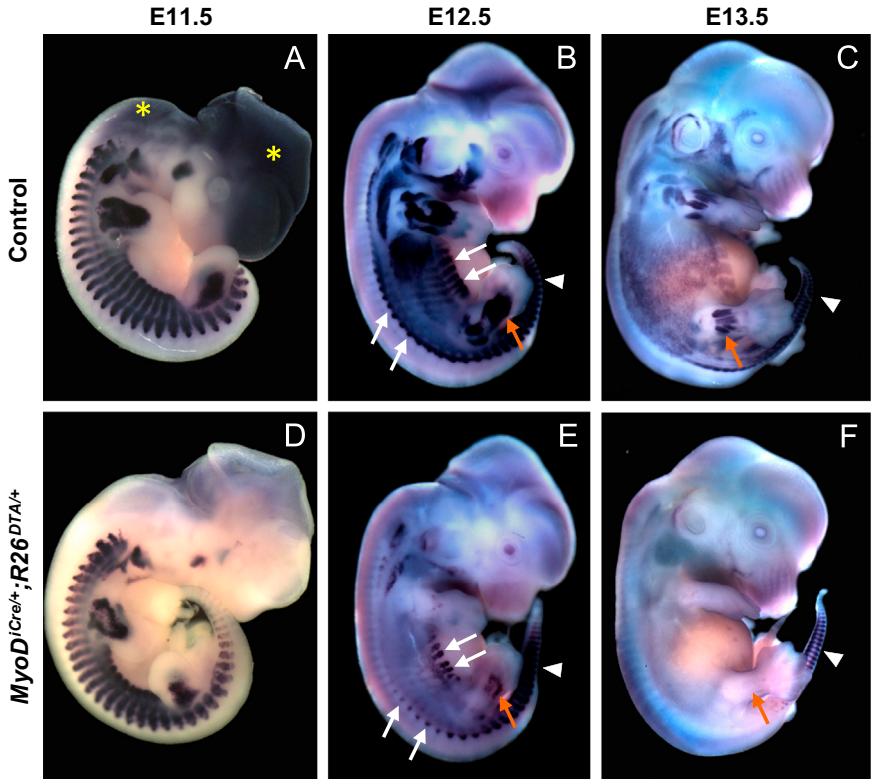

Fig. 3. Whole mount in situ hybridization for MyoD transcripts in control and $MyoD^{iCre/+}$;$R26^{DTA/+}$ embryos. (A, D) E11.5 control and DTA embryos showed a similar pattern and apparent abundance of MyoD transcripts, except for a modest reduction in the limb buds of DTA embryos. Staining in the head and dorsal neck in A is background staining (asterisks). (B, E) By E12.5, MyoD transcripts in DTA embryos were dramatically reduced in developing muscle-forming regions of the head, trunk and limbs, with strong staining primarily restricted to the dorsal- and ventral-most interlimb body wall muscles (white arrows), the hindlimbs (orange arrow), and the myotomes of the tail (arrowhead). Similar areas are marked in control and DTA embryos. (C, F) By E13.5, staining for MyoD transcripts was undetectable except for faint staining in the hindlimbs (orange arrows) and in the most posterior tail somites (arrowheads).

limbs (Fig. 4E). We also assessed muscle differentiation at E16.5 as a sensitive endpoint assay for the presence and expansion of myogenic progenitor cells, which could represent either a small, persistent, $MyoD^{low}$ population that expressed insufficient Cre to recombine the DTA allele, or a distinct population of MyoD-negative cells. As assessed by MyHC expression and histological observations (unpublished observations), differentiating skeletal muscle was undetectable at E16.5 (Fig. 4G, H), indicating either the complete loss of myogenic progenitor populations or their inability to rescue myogenesis. Qualitatively similar results were obtained using an attenuated form of DTA (R-DTA; Wu et al., 2006; Haldar et al., 2008), although the time-course of cell ablation was delayed and a few scattered MyHC+ cells persisted at E16.5 (Fig. S3).

Myf-5+ myogenic progenitors are lost in MyoD lineage ablated embryos

Immunofluorescence and whole mount in situ hybridization were used to determine whether Myf-5+ myogenic progenitors persist in $MyoD^{iCre/+}R26^{DTA/+}$ embryos. Myf-5 immunoreactivity was lost over a time course similar to that of MyoD (Fig. 2) and MyHC (Fig. 4). E10.5 embryos showed a modest reduction in Myf-5 staining in hypaxial myotomes and some embryos also showed a reduction in staining of the forelimb buds (Fig. 5A, B), although the latter was a less consistent finding and the degree of reduction was variable. The loss of Myf-5 immunoreactivity was pronounced by E11.5 (Fig. 5C, D) and essentially complete by E12.5 (Fig. 5E, F). Analysis of later stage embryos did not reveal an emergence and expansion of Myf5+ progenitors, in contradistinction to Myf-5 lineage ablated embryos, in which compensatory expansion of MyoD+ progenitors was observed (Gensch et al., 2008; Haldar et al., 2008). The loss of Myf-5 mRNA closely paralleled the loss of MyoD transcripts described above (Fig. 6). A modest reduction in Myf-5 mRNA was observed in the forelimb buds at E11.5 (Fig. 6A, D), followed by a sharp decline throughout the body by E12.5, and loss of detectable Myf-5 transcripts by E13.5, except in the developmentally youngest myotomes at the tip of the tail (Fig. 6C, F). Collectively, the data presented thus far argue against the existence of a distinct, MyoD-negative population of myogenic progenitors.

Persistence of myogenic progenitors following ablation of differentiating muscle

We next addressed whether cell non-autonomous effects could account for the apparent absence of MyoD-negative progenitors. For example, DTA-mediated disruption of the normal structural and signaling environment caused by the loss of MyoD+ progenitors and differentiating muscles might indirectly lead to the death or fate change of MyoD-independent progenitors. We sought to test this possibility by approximating these disruptive changes in the developing muscle beds by specifically directing DTA expression to differentiating muscles without directly affecting muscle progenitors. For these experiments, we used ACTA1Cre mice, in which the α-skeletal actin promoter drives Cre expression (Miniou et al., 1999), and evaluated the efficiency of ablation of differentiating muscle, and the presence of muscle progenitors. α-skeletal actin expression is initiated within 12 h of MyoD in hypaxial muscles (approximately E10.5 and E11 in the forelimb buds for MyoD and α-skeletal actin, respectively; Sassoon et al., 1988; Tajbakhsh et al., 1997; Chen and Goldhamer, 2004), and the Cre-

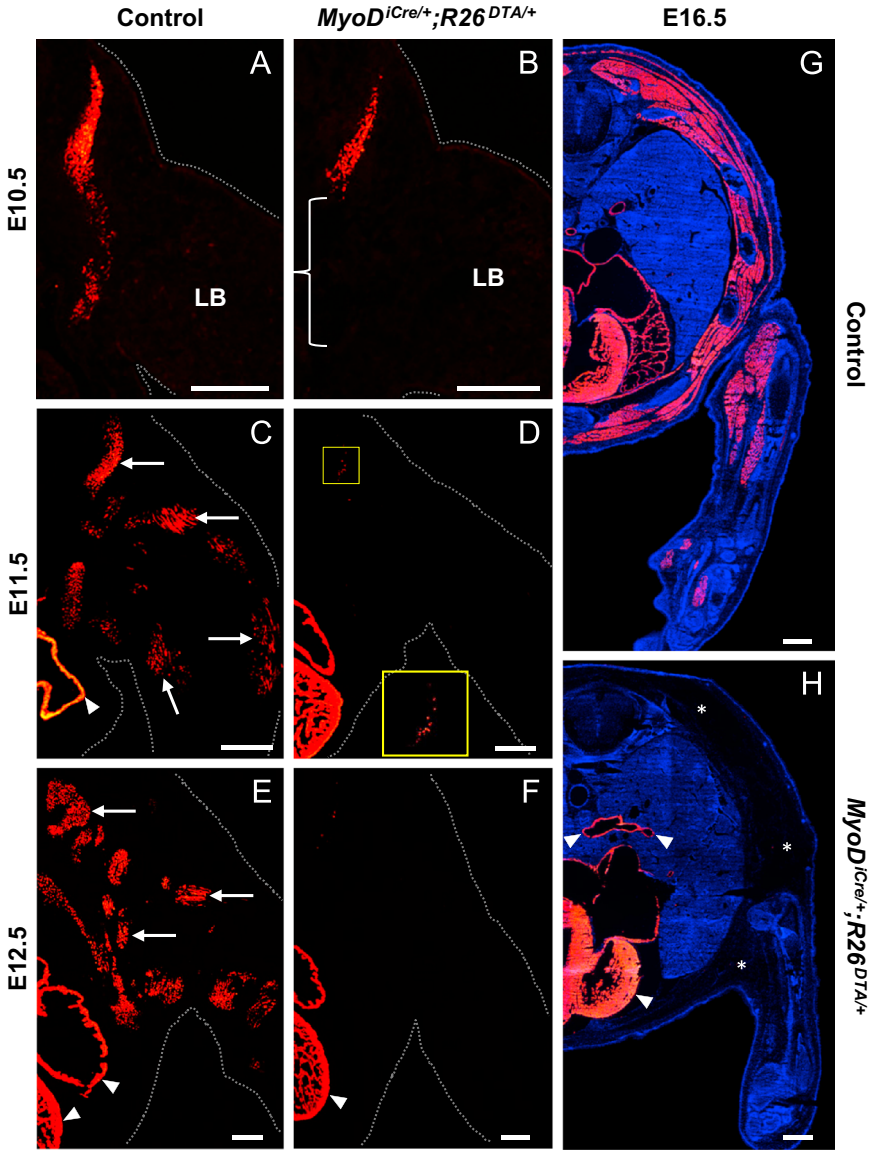

Fig. 4. Loss of MyHC expression in MyoD lineage-ablated embryos. (A, B) Loss of MyHC immunoreactivity was first observed in hypaxial myotomes at forelimb and interlimb levels at E10.5 (bracket). (C, D) MyHC immunoreactivity in E11.5 $MyoD^{iCre/+}$;$R26^{DTA/+}$ embryos was restricted to a few scattered cells in the trunk (D; small yellow box). This area is enlarged in the inset to show MyHC+ cells. Examples of MyHC+ muscle masses in the trunk and forelimb of a control embryo (C) are shown at the arrows. MyHC staining in the forelimb buds of this control embryo (C) was greater than typical for this stage. The heart stained intensively with mAb MF20 (arrowhead), which recognizes all forms of sarcomeric myosin. (E, F) By E12.5, MyHC staining of skeletal muscle was abolished. MyHC expression in the heart (arrowheads) serves as a positive internal control for staining. (G, H) Differentiated skeletal muscle was absent in E16.5 DTA embryos, demonstrating the lack of functional MyoD lineage-independent compensatory pathways for muscle differentiation in $MyoD^{iCre/+}$;$R26^{DTA/+}$ embryos. MyHC staining in DTA embryos was restricted to the heart and certain larger vessels of the circulatory system (examples at arrowheads). Dark areas in H are fluid filled spaces devoid of tissue (asterisks), which is common in late stage embryos lacking skeletal muscle. Panels G and H were counterstained with DAPI. Panels C, D, G, and H are assembled composites of multiple images. Scale bars represent 200 μm in A–F, and 400 μm in G and H.

dependent GFP reporter, $R26^{NG}$ (Yamamoto et al., 2009), is expressed in the expected muscle specific pattern in ACTA1Cre embryos at E11.5 and E12.5 (Fig. S4). In ACTA1Cre;$R26^{DTA/+}$ embryos, MyHC was undetectable at E11.5 and E12.5 (Fig. 7A, B, E, F), and remained undetectable through E16.5 (data not shown), demonstrating that differentiating muscle was efficiently targeted for DTA expression. MyoD-expressing progenitors persisted through E12.5 in ACTA1Cre;$R26^{DTA/+}$ embryos, and only a minor reduction in the number of MyoD+ cells was observed (Fig. S5). In contrast to MyoD lineage-ablated embryos, targeting of differentiating muscle for ablation had little effect on Myf-5 expression at E11.5 (Fig. 7C, D). Myf-5+ cells were also abundant at E12.5, although their number was reduced relative to control embryos (Fig. 7G, H). Co-expression of Myf-5 in differentiating, DTA-expressing, cells likely contributed to the loss of Myf-5 immunoreactivity, as overlap in Myf-5 and MyHC staining was observed in control embryos at E12.5 (Fig. S6). We observed, however, a substantial reduction in the apparent level of Myf-5 expression (Fig. 7G, H), which may indicate that the maintenance of Myf-5 expression is dependent on the muscle environment, as has been shown for Pax7 (Kassar-Duchossoy et al., 2005). The persistence of Myf-5+ progenitors in ACTA1Cre;$R26^{DTA/+}$ embryos during the time frame in which essentially all Myf-5+ progenitors are lost in $MyoD^{iCre/+}R26^{DTA/+}$ embryos indicates that cell non-autonomous effects cannot explain the rapid loss of Myf-5+ cells in MyoD lineage-ablated embryos. This is consistent with the capacity of myoblasts to survive, proliferate and undergo myogenic differentiation in the setting of widespread DTA-mediated disruption of the muscle beds by ablation of Myf-5+ progenitors (Gensch et al., 2008; Haldar et al., 2008).

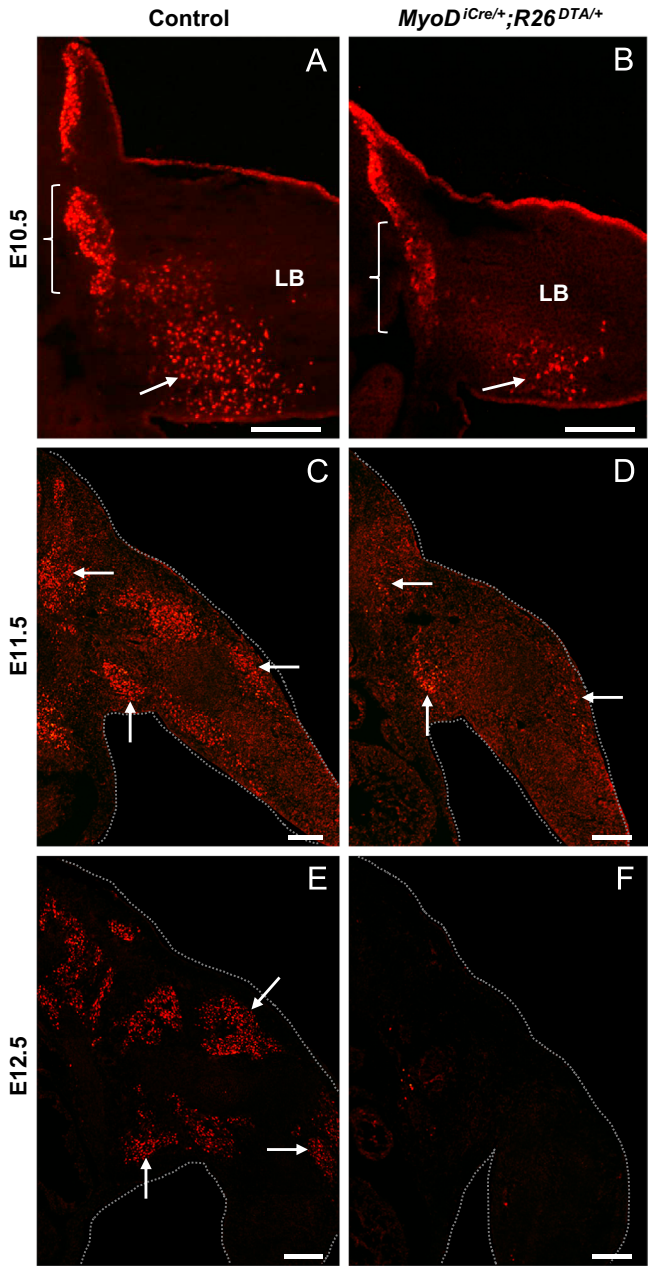

Fig. 5. Loss/translational inhibition of Myf-5+ progenitors in MyoD lineage-ablated embryos. (A, B) As with MyoD protein expression, partial loss of Myf-5 immunoreactivity was first observed at E10.5 in the forelimb buds and in hypaxial myotomes at limb (bracket) and inter-limb levels at E10.5. (C, D) By E11.5, Myf-5 immunoreactivity in $MyoD^{iCre/+}$;$R26^{DTA/+}$ embryos (D) was restricted to a few scattered cells in the trunk and limb buds (arrows). Examples of Myf-5+ muscle masses in the trunk and forelimb bud of a control embryo (C) are shown at the arrows. (E, F) By E12.5, Myf-5 staining of skeletal muscle in MyoD lineage-ablated embryos (F) was essentially abolished. Examples of Myf-5+ muscle masses in the trunk and forelimb of a control embryo (E) are shown at the arrows. E11.5 and E12.5 panels are assembled composites of multiple images. Scale bars represent 200 μm.

Pax7+ satellite cell progenitors are lost in MyoD lineage ablated embryos

Satellite cells are the major stem cell responsible for muscle regeneration (Zammit, 2008; Lepper et al., 2011; Murphy et al., 2011; McCarthy et al., 2011). We previously showed that satellite cells are derived from *MyoD*-expressing progenitors, although MyoD function is not required in these progenitors for satellite cell development (Kanisicak et al., 2009). To address whether other embryonic cell populations can serve as satellite cell progenitors when MyoD+ cells are ablated, we assessed Pax7 expression in MyoD lineage-ablated embryos. Markers exclusive to satellite cell progenitors are not available, and Pax7 marks progenitors of both satellite cells and myogenic cells engaged in ongoing myogenesis (Relaix et al., 2004, 2005; Kassar-Duchossoy et al., 2005; Hutcheson et al., 2009; Lepper and Fan, 2010). In the limb buds, where most investigations have focused, Pax7 is first activated at approximately E11.5 in a subset of Pax3+ progenitors (Relaix et al., 2004, 2005; Kassar-Duchossoy et al., 2005; Hutcheson et al., 2009), which are MRF-negative as they migrate from the hypaxial dermomyotome of limb-level somites and enter the developing limbs by E10.5 (Bober et al., 1994; Relaix et al., 2004). As expected, Pax3+ cells were abundant in the premuscle masses of E10.5 forelimb buds (Fig. 8A). We also noted the presence of a few scattered Pax7+ cells at this stage (Fig. 8C). No consistent reduction in Pax3 or Pax7 staining was observed in forelimb buds of $MyoD^{iCre/+}$;$R26^{DTA/+}$ embryos at E10.5 (Fig. 8A–D), which is prior to detectable $MyoD^{iCre/+}$-dependent gene expression (Fig. 2A; Kanisicak et al., 2009). By E12.5, however, when the major muscle groups of the limbs and trunk are marked by robust Pax7 expression in control embryos (Fig. 8E), Pax7 staining in MyoD lineage-ablated embryos was restricted to a small number of individual or clustered cells, (Fig. 8F), consistent with the view that the great majority of Pax7+ progenitors express MyoD by E12.5. Pax7+ progenitors were not observed in $MyoD^{iCre/+}$;$R26^{DTA/+}$ embryos at E16.5 (Fig. 8I, J), the approximate stage at which satellite cells can be anatomically identified as Pax7+ cells lying beneath the nascent muscle fiber basal lamina (Kassar-Duchossoy et al., 2005; Relaix et al., 2005; Lepper and Fan, 2010). Importantly, Pax7+ cells were abundant in the muscle forming areas of the limbs and trunk of E12.5 ACTA1Cre;$R26^{DTA/+}$ embryos (Fig. 8G, H), and Pax7+ progenitors persisted through E16.5 (Fig. 8K–N), despite the absence of differentiating skeletal muscle. We note, however, that the number of Pax7+ cells was substantially reduced at both stages relative controls, which might reflect a need for paracrine signaling by differentiating skeletal muscle to maintain Pax7 expression (Kassar-Duchossoy et al., 2005). Collectively, these data show that cell-non-autonomous effects cannot explain the rapid and complete loss of Pax7 immunoreactivity in MyoD lineage-ablated embryos, although the absence of differentiating muscle probably contributed to the reduction in Pax7 immunoreactivity.

Discussion

Defining the sizes and interrelationship of MRF-expressing myogenic populations is essential for a complete understanding of the regulatory circuitry controlling myogenic lineage determination and the compensatory mechanisms that render each factor individually dispensable for skeletal muscle development. In this study, we used DTA-mediated cell ablation, together with immunofluorescence analyses and lineage tracing, to investigate the interrelationship of MyoD+ and Myf-5+ myogenic populations, and to specifically test whether MyoD+ progenitors are essential for muscle development. In stark contrast to the phenotype of Myf-5 lineage-ablated embryos, in which myogenesis is delayed but shows a full recovery by fetal stages (Gensch et al., 2008; Haldar et al., 2008), loss of MyoD-expressing progenitors resulted in the cessation of myogenesis, as demonstrated by the complete loss of differentiating muscle subsequent to $MyoD^{iCre}$-dependent activation of DTA expression. Importantly, Myf-5+ progenitors were lost concomitant with the loss of MyoD+ progenitors, suggesting that all Myf-5+ myogenic cells express MyoD. This conclusion is supported by our analysis of Myf-5 protein expression in E12.5 $MyoD^{iCre/+}$;$R26^{NG/+}$ embryos, in which only rare

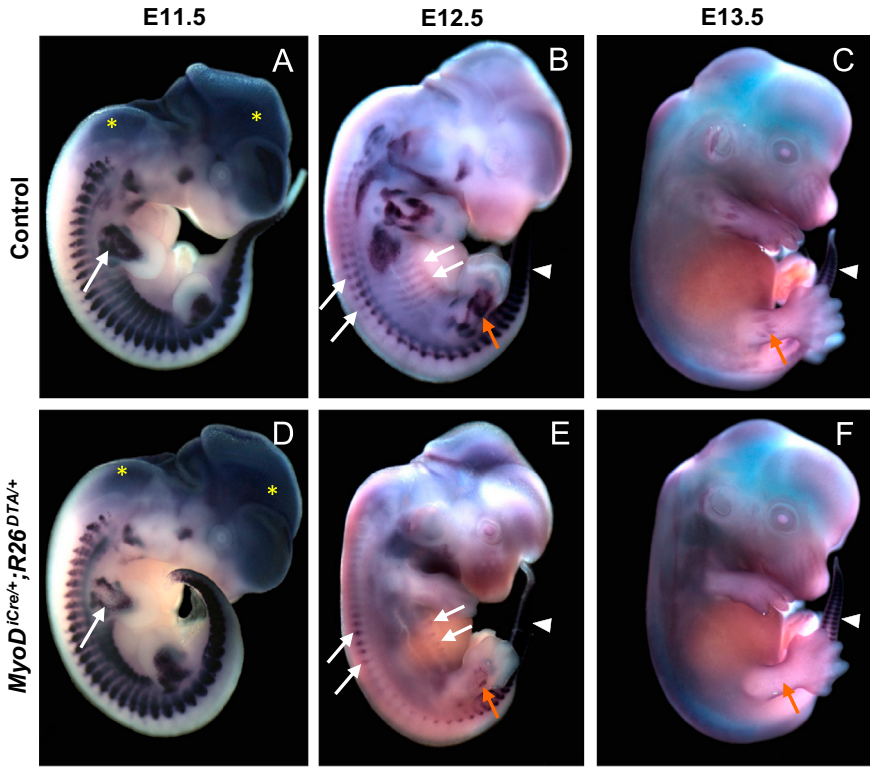

Fig. 6. Whole mount in situ hybridization for Myf-5 transcripts in control and MyoD lineage-ablated embryos. (A, D) At E11.5, clear effects of DTA expression were restricted to the forelimb buds (arrows). Staining in the head and dorsal neck in (A) and (D) is background staining (asterisks). (B, E) By E12.5, Myf-5 transcripts in *MyoD*$^{iCre/+}$;*R26*$^{DTA/+}$ embryos were markedly reduced in muscle-forming regions of the head, trunk and limbs, with staining primarily restricted to the dorsal- and ventral-most interlimb body wall muscles (white arrows), the hindlimbs (orange arrows), and the myotomes of the tail (arrowheads). Similar areas are marked in control and *MyoD*$^{iCre/+}$;*R26*$^{DTA/+}$ embryos. (C, F) By E13.5, staining for Myf-5 transcripts was undetectable except for very faint staining in the hindlimbs (orange arrows), and in the most posterior tail somites (arrowheads).

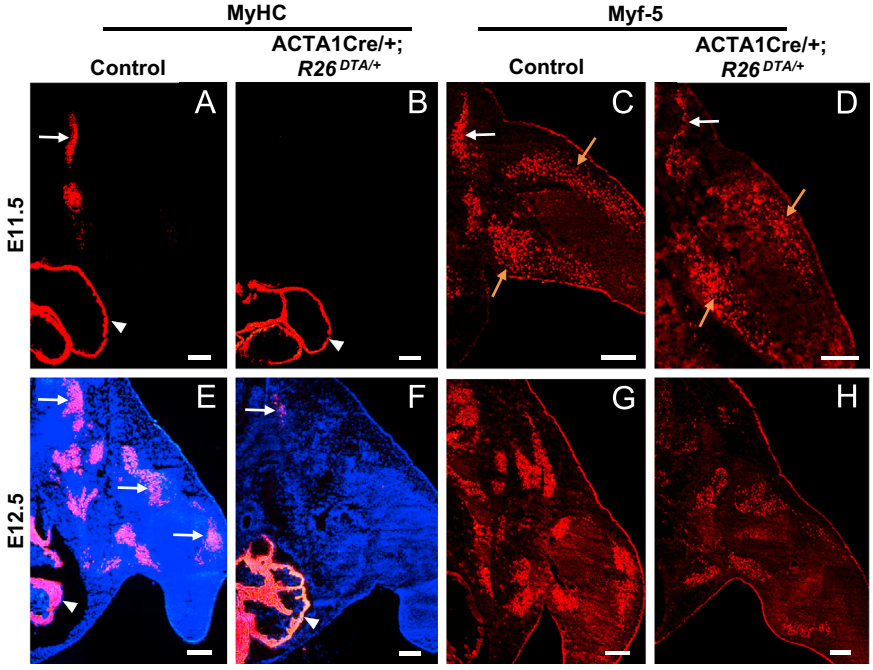

Fig. 7. Persistence of Myf-5+ progenitors when differentiating skeletal muscle was targeted for DTA-mediated ablation. (A, B, E, F) Except for rare cells (arrow, F), MyHC staining is completely lost at E11.5 and E12.5 in ACTA1Cre;*R26*$^{DTA/+}$ embryos. Arrow in A, MyHC+ myotome. Arrows in E, examples of MyHC+ muscle groups in the trunk and limb. The heart is robustly MyHC+ in both control and experimental embryos (arrowheads in A, B, E, and F). (C, D) Myf-5 staining in the myotomes of limb-level (white arrows) and interlimb somites is reduced in ACTA1Cre;*R26*$^{DTA/+}$ embryos at E11.5, whereas staining of the dorsal and ventral premuscle masses (orange arrows) of the forelimb buds is not appreciably affected. (G H) At E12.5, the majority of Myf-5+ progenitors persisted, although the immunofluorescence signal is reduced relative to controls. Panels E and F were counterstained with DAPI. Panels B, C, D, G, and H are assembled composites of multiple images. Scale bars represent 200 μm.

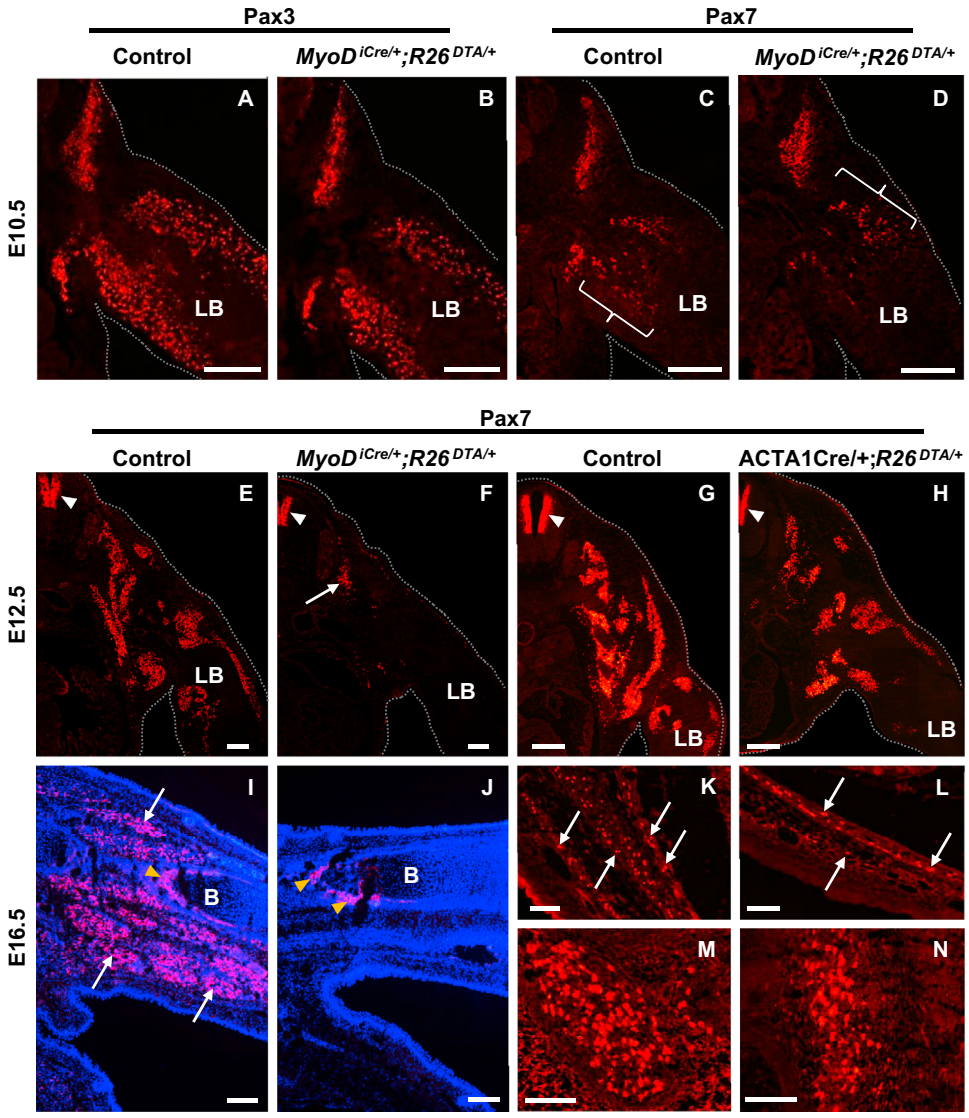

Fig. 8. Loss/translational inhibition of Pax7+ progenitors in MyoD lineage-ablated embryos. (A–D) Expression of Pax3 and Pax7 were not appreciably affected in $MyoD^{iCre/+}$; $R26^{DTA/+}$ embryos at E10.5. Weak Pax7 staining (brackets) in the proximal forelimb buds is first detected at this stage. (E, F) Very few Pax7+ cells are detectable at E12.5 in MyoD lineage-ablated embryos. A small cluster of Pax7+ cells in the trunk of this $MyoD^{iCre/+}$;$R26^{DTA/+}$ embryo (F) is shown at the arrow. Pax7 staining of the neural tube (arrowheads) serves as a positive internal control for staining. Pax7 is robustly expressed in muscle groups of the trunk and limbs in control embryos (E). (G, H) Many Pax7+ cells persisted at E12.5 in ACTA1Cre; $R26^{DTA/+}$ embryos (H), although their number was reduced relative to controls (G). Arrowheads, Pax7 staining of the neural tube. (I, J) Longitudinal sections through the forelimbs of control (I) and $MyoD^{iCre/+}$;$R26^{DTA/+}$ (J) embryos at E16.5. Pax7+ cells were abundant in the muscle beds of control forelimbs (arrows), but were absent in MyoD lineage-ablated forelimbs, which lack differentiating skeletal muscle (see Fig. 4H). Yellow arrowheads, autofluorescence associated with the periosteum of the developing bone (B). (K, L) Transverse sections through the ventral body wall of control (K) and ACTA1Cre; $R26^{DTA/+}$ (L) E16.5 embryos. Pax7+ progenitors were readily apparent, but reduced in number, in ACTA1Cre; $R26^{DTA/+}$ embryos. Numbers of Pax7+ cells varied considerably between sections and this is an "average" example. (M, N) Longitudinal sections through the distal hindlimbs of control and ACTA1Cre;$R26^{DTA/+}$ embryos at E16.5. Pax7+ cells were abundant in the muscle beds of control embryos (M). Many Pax7+ progenitors persisted in the limbs of ACTA1Cre;$R26^{DTA/+}$ embryos (N) despite the absence of differentiating skeletal muscle, although their numbers were consistently reduced relative to controls. Panels I and J were counterstained with DAPI. Panels E–H are assembled composites of multiple images. LB, limb bud. Scale bars represent 200 μm in A–F and I–J, 400 μm in G and H, 100 μm in K–N.

Myf-5+ cells were observed that were not lineage-marked for *MyoD* expression or did not express detectable MyoD protein. As embryos lacking both MyoD and Myf-5 undergo limited and transient embryonic myogenesis, which is directed by the related factor, *Mrf4* (Kassar-Duchossoy et al., 2004), we attempted to evaluate the possible presence of a significant pool of Mrf4+MyoD– progenitors. These experiments, however, were inconclusive because of the poor quality of immunofluorescence staining with commercially available antibodies against Mrf4 (data not shown). However, >98% of Pax7+ progenitors in the hindlimbs at E13.5 were lineage marked by the historical or ongoing expression of MyoD (unpublished observations), arguing against the existence of a distinct Mrf4+MyoD– progenitor population. Clearly, if a very small Mrf4+MyoD– population exists, it is incapable of supporting a detectable level of myogenesis in MyoD lineage-ablated embryos subsequent to the initial formation of the myotome, which is under the genetic control of *Myf-5* (Braun et al., 1992; Tajbakhsh et al., 1997) and *Mrf4* (Kassar-Duchossoy et al., 2004), prior to the induction of *MyoD*.

The present study was not designed to distinguish whether Myf-5 is co-expressed with MyoD in all myogenic cells, or whether Myf-5+ cells represent a subset of the MyoD+ progenitor pool. Results of Cre/loxP-dependent DTA lineage ablation using $Myf\text{-}5^{Cre}$ alleles support the existence of a functionally significant pool of Myf-5–MyoD+ progenitors (Gensch et al., 2008; Haldar et al., 2008). However, the efficiency of Cre-mediated recombination is

highly dependent on both the Cre driver and the floxed target allele (Nagy, 2000; Lewandoski, 2001; Ma et al., 2008; Sambasivan et al., 2013), and it is difficult to exclude the possibility that the apparent presence of Myf-5-negative cells was due to incomplete Cre recombination among Myf-5-expressing progenitors (also see Sambasivan et al., 2013). Whereas the loss of Cre-dependent reporter gene expression in DTA embryos was clearly shown (Gensch et al., 2008; Haldar et al., 2008), these data did not rule out the existence of Myf-5+ cells in which both the floxed reporter and DTA alleles remained unrecombined because of insufficient levels of Cre. Given these considerations, the possible existence of a distinct population of Myf-5-negative myogenic progenitors requires further investigation. Nevertheless, the recovery of myogenesis following ablation of most Myf-5-expressing progenitors (Gensch et al., 2008; Haldar et al., 2008) dramatically demonstrates the marked compensatory capacity of developing skeletal muscle. Determining whether rescue of myogenesis in these embryos is driven by expansion of MRF+ myoblasts, more primitive, Pax+MRF– progenitors, or both, will provide important insights into cellular mechanisms that drive this regulative capacity.

While we interpret the loss of Myf-5 expression in $MyoD^{iCre/+}$;$R26^{DTA/+}$ embryos as evidence for co-expression of MyoD in the great majority of Myf-5-expressing progenitors cells outside of the early myotome, it is important to consider other possible explanations. For example, we cannot exclude *a priori* the existence of a small, distinct Myf-5+MyoD– progenitor population that was lost only after fusion to MyoD+, dying myoblasts. Notwithstanding the unlikelihood that DTA-expressing myoblasts remain fusion competent, this scenario is inconsistent with the fact that Myf-5 immunoreactivity is almost completely lost by E11.5, a stage at which the developing muscle beds are comprised predominantly of mononuclear progenitors. Further, any minor role that fusion might play in the loss of progenitor cells did not prevent rescue of myogenesis by MyoD+ progenitors following ablation of Myf-5-expressing cells (Gensch et al., 2008; Haldar et al., 2008).

We also used ACTA1Cre mice (Miniou et al., 1999) to test whether cell non-autonomous effects could explain the loss of Myf-5+ progenitors by assessing the consequences on progenitor populations when DTA expression was directed specifically to differentiating skeletal muscles. Strikingly, while Myf-5 expression was essentially absent by E12.5 in MyoD lineage-ablated embryos, large numbers of Myf-5+ progenitors persisted through E12.5 in ACTA1Cre;$R26^{DTA/+}$ embryos. These data strongly suggest that the rapid loss of Myf-5+ myogenic progenitors in $MyoD^{iCre/+}$;$R26^{DTA/+}$ embryos was largely due to DTA expression in those progenitors, and cannot be explained by cell non-autonomous effects. The ability of MyoD+ cells to rescue myogenesis in Myf-5 lineage-ablated embryos (Gensch et al., 2008; Haldar et al., 2008) also shows that widespread disruption of the muscle environment is compatible with myogenic progenitor cell survival, expansion and differentiation. Nevertheless, we did observe a reduction in Myf-5+ progenitor numbers and expression levels in ACTA1Cre;$R26^{DTA/+}$ muscle beds relative to control embryos, consistent with some contribution of the muscle environment on progenitor cell loss or Myf-5 expression (see below). We showed, however, that much of the loss of Myf-5 immunoreactivity in ACTA1Cre;$R26^{DTA/+}$ embryos at E12.5 can be accounted for by the loss (or translational inhibition within) of nascent myocytes and muscle fibers in which Myf-5 is normally expressed.

Pax7 is an accepted and widely utilized marker for satellite cells and their progenitors (Seale et al., 2000; Kassar-Duchossoy et al., 2005; Relaix et al., 2005; Bosnakovski et al., 2008) and is an early marker of myogenic lineage restriction in the limbs (Hutcheson et al., 2009; Lepper and Fan, 2010). We showed that Pax7 expression is lost in $MyoD^{iCre/+}$;$R26^{DTA/+}$ embryos, consistent with previous lineage analyses, which demonstrated that satellite cell progenitors express *MyoD* prior to birth (Kanisicak et al., 2009). An unexpected finding of the current study, however, was the rapid loss, by E12.5, of essentially all Pax7+ cells. While existing markers do not allow the specific identification of Pax7+ satellite cell progenitors among the Pax7+ myogenic population, conditional lineage labeling with a $Pax7^{CreER}$ driver ($Pax7^{CE}$) demonstrated the emergence of Pax7+ satellite cell progenitors by E9.5 and E11.5 in certain trunk and limb muscles, respectively (Lepper and Fan, 2010). As such, the loss of Pax7 immunoreactivity in MyoD lineage-ablated embryos suggests that *MyoD* is activated in at least some, and perhaps all, satellite cell progenitors by E12.5. Accordingly, conditional lineage tracing revealed the emergence of MyoD+ satellite cell progenitors by E12.5, although a relatively low Cre recombination efficiency precluded precise quantification (unpublished observations). Importantly, however, immunohistochemical studies have shown that cells expressing Pax3, Pax7 or both markers, but negative for MRF expression (Pax+MRF–), persist through fetal stages (Kassar-Duchossoy et al., 2005; Relaix et al., 2005). Whereas the presence of progenitors with this marker profile may reflect, in part, the dynamic expression and rapid turnover of MyoD and Myf-5 (Kitzmann et al., 1998; Thayer et al., 1989; Carnac et al., 1998; Kanisicak et al., 2009), we cannot exclude the possibility that MyoD+ satellite cell progenitors continually emerge from a persistent Pax+MRF– pool. This scenario can be reconciled with the present DTA ablation data if *MyoD* expression is activated prior to or concomitant with Pax7 in some Pax3+ progenitors, or if Pax7+ cells generated after E12.5 escaped detection because of the rapid, subsequent, activation of $MyoD^{iCre}$-dependent DTA expression. In fact, MyoD expression precedes Pax7 expression in limb muscle progenitors (Tajbakhsh et al., 1997; Chen and Goldhamer, 2004; Relaix et al., 2004; unpublished observations), supporting the former mechanism. Disruption of the muscle environment also probably contributed to the loss of Pax7 immunoreactivity, since Pax7 staining was reduced when differentiating cells, which do not express Pax7 (Kassar-Duchossoy et al., 2005; Relaix et al., 2005; Olguin et al., 2007; Dey et al., 2011), were targeted for ablation. While Pax7+ cells are resistant to apoptosis in muscle-deficient embryos, paracrine signaling by differentiating muscle may regulate the maintenance of Pax7 expression (Kassar-Duchossoy et al., 2005). Nevertheless, the dramatic difference in the timing and extent of loss of Pax7 immunoreactivity in $MyoD^{iCre/+}$;$R26^{DTA/+}$ and ACTA1Cre;$R26^{DTA/+}$ embryos is consistent with the notion that most Pax7+ progenitors express *MyoD*, at least transiently, by E12.5.

Satellite cell progenitors of the limb share a number of fundamental properties with fetal myoblasts or their progenitors, including their origin from the dermomyotome of limb-level somites (Armand et al., 1983; Gros et al., 2005; Schienda et al., 2006; Lepper and Fan, 2010), sequential activation of Pax3 and Pax7 expression (Bober et al., 1994; Relaix et al., 2004; Hutcheson et al., 2009) and expression of *MyoD* (Kanisicak et al., 2009; present study), *Myf-5* (Biressi et al., 2013) and *Mrf4* (Sambasivan et al., 2013). Indeed, no molecular properties unique to satellite cell progenitors have been identified, and it remains unclear whether satellite cell progenitors represent a distinct, MyoD-expressing lineage, or how and when they are partitioned from myogenic populations engaged in embryonic and fetal myogenesis. In this regard, recent data have demonstrated microRNA-mediated translational inhibition of Myf-5 mRNA in adult quiescent satellite cells, a regulatory mechanism that may prevent premature activation of the myogenic program (Crist et al., 2012). Importantly, Cre-based lineage analyses and DTA ablation rely on transcriptional output from a locus of interest and do not address whether the cognate protein is expressed. Whereas all Cre protein-positive cells

of the forelimb muscle beds of *MyoD*^{iCre} mice were positive for MyoD protein at E16.5 (Kanisicak et al., 2009), and the great majority of MyoD lineage-labeled cells at E12.5 expressed MyoD protein (present study), markers specific to satellite cell progenitors are required to formally demonstrate expression of MyoD protein in this population. If MyoD protein is expressed in satellite cell progenitors during embryonic development, it will be important to determine how these progenitors are prevented from engaging in ongoing embryonic and fetal myogenesis, and whether expression of this key lineage-determining factor is sufficient for stable myogenic programming of satellite cells.

Acknowledgments

We thank Shoko Yamamoto for technical assistance, William O'Hara for advice on immunofluorescence, Youfen Sun for assistance with mouse care, Dr. Carol Norris for training on the confocal microscope, and members of the Goldhamer lab for helpful suggestions throughout the course of this work. The Edward A. Khairallah Fellowship provided partial summer support to W. M.W. This work was supported, in part, by a Grant from NIAMS to D.J.G.

Appendix A. Supplementary material

Supplementary data associated with this article can be found in the online version at http://dx.doi.org/10.1016/j.ydbio.2013.09.012.

References

Armand, O., Boutineau, A.M., Mauger, A., Pautou, M.P., Kieny, M., 1983. Origin of satellite cells in avian skeletal muscles. Arch. Anat. Microsc. Morphol. Exp. 72, 163–181.
Bader, D., Masaki, T., Fischman, D.A., 1982. Immunochemical analysis of myosin heavy chain during avian myogenesis in vivo and in vitro. J. Cell Biol. 95, 763–770.
Biressi, S., Bjornson, C.R., Carlig, P.M., Nishijo, K., Keller, C., Rando, T.A., 2013. Myf5 expression during fetal myogenesis defines the developmental progenitors of adult satellite cells. Dev. Biol. 379, 195–207.
Bober, E., Franz, T., Arnold, H.H., Gruss, P., Tremblay, P., 1994. Pax-3 is required for the development of limb muscles: a possible role for the migration of dermomyotomal muscle progenitor cells. Development 120, 603–612.
Bosnakovski, D., Xu, Z., Li, W., Thet, S., Cleaver, O., Perlingeiro, R.C., Kyba, M., 2008. Prospective isolation of skeletal muscle stem cells with a Pax7 reporter. Stem Cells 26, 3194–3204.
Braun, T., Rudnicki, M.A., Arnold, H.H., Jaenisch, R., 1992. Targeted inactivation of the muscle regulatory gene Myf-5 results in abnormal rib development and perinatal death. Cell 71, 369–382.
Carnac, G., Primig, M., Kitzmann, M., Chafey, P., Tuil, D., Lamb, N., Fernandez, A., 1998. RhoA GTPase and serum response factor control selectively the expression of MyoD without affecting myf5 in mouse myoblasts [in process citation]. Mol. Biol. Cell 9, 1891–1902.
Chen, J.C., Goldhamer, D.J., 2004. The core enhancer is essential for proper timing of MyoD activation in limb buds and branchial arches. Dev. Biol. 265, 502–512.
Chen, J.C., Mortimer, J., Marley, J., Goldhamer, D.J., 2005. MyoD-cre transgenic mice: a model for conditional mutagenesis and lineage tracing of skeletal muscle. Genesis 41, 116–121.
Chen, J.C., Ramachandran, R., Goldhamer, D.J., 2002. Essential and redundant functions of the MyoD distal regulatory region revealed by targeted mutagenesis. Dev. Biol. 245, 213–223.
Cossu, G., Kelly, R., Tajbakhsh, S., Di Donna, S., Vivarelli, E., Buckingham, M., 1996. Activation of different myogenic pathways: myf-5 is induced by the neural tube and MyoD by the dorsal ectoderm in mouse paraxial mesoderm. Development 122, 429–437.
Crist, C.G., Montarras, D., Buckingham, M., 2012. Muscle satellite cells are primed for myogenesis but maintain quiescence with sequestration of Myf5 mRNA targeted by microRNA-31 in mRNP granules. Cell Stem Cell 11, 118–126.
Dey, B.K., Gagan, J., Dutta, A., 2011. miR-206 and -486 induce myoblast differentiation by downregulating Pax7. Mol. Cell. Biol. 31, 203–214.
Faerman, A., Goldhamer, D.J., Puzis, R., Emerson Jr., C.P., Shani, M., 1995. The distal human myoD enhancer sequences direct unique muscle-specific patterns of lacZ expression during mouse development. Dev. Biol. 171, 27–38.
Gensch, N., Borchardt, T., Schneider, A., Riethmacher, D., Braun, T., 2008. Different autonomous myogenic cell populations revealed by ablation of Myf5-expressing cells during mouse embryogenesis. Development 135, 1597–1604.
Goldhamer, D.J., Brunk, B.P., Faerman, A., King, A., Shani, M., Emerson Jr., C.P., 1995. Embryonic activation of the myoD gene is regulated by a highly conserved distal control element. Development 121, 637–649.
Goldhamer, D.J., Faerman, A., Shani, M., Emerson Jr., C.P., 1992. Regulatory elements that control the lineage-specific expression of myoD. Science 256, 538–542.
Gros, J., Manceau, M., Thome, V., Marcelle, C., 2005. A common somitic origin for embryonic muscle progenitors and satellite cells. Nature 435, 954–958.
Haldar, M., Karan, G., Tvrdik, P., Capecchi, M.R., 2008. Two cell lineages, myf5 and myf5-independent, participate in mouse skeletal myogenesis. Dev. Cell 14, 437–445.
Henrique, D., Adam, J., Myat, A., Chitnis, A., Lewis, J., Ish-Horowicz, D., 1995. Expression of a Delta homologue in prospective neurons in the chick. Nature 375, 787–790.
Hutcheson, D.A., Zhao, J., Merrell, A., Haldar, M., Kardon, G., 2009. Embryonic and fetal limb myogenic cells are derived from developmentally distinct progenitors and have different requirements for beta-catenin. Genes Dev. 23, 997–1013.
Ivanova, A., Signore, M., Caro, N., Greene, N.D., Copp, A.J., Martinez-Barbera, J.P., 2005. In vivo genetic ablation by Cre-mediated expression of diphtheria toxin fragment A. Genesis 43, 129–135.
Kablar, B., Krastel, K., Ying, C., Asakura, A., Tapscott, S.J., Rudnicki, M.A., 1997. MyoD and Myf-5 differentially regulate the development of limb versus trunk skeletal muscle. Development 124, 4729–4738.
Kanisicak, O., Mendez, J.J., Yamamoto, S., Yamamoto, M., Goldhamer, D.J., 2009. Progenitors of skeletal muscle satellite cells express the muscle determination gene, MyoD. Dev. Biol. 332, 131–141.
Kassar-Duchossoy, L., Gayraud-Morel, B., Gomes, D., Rocancourt, D., Buckingham, M., Shinin, V., Tajbakhsh, S., 2004. Mrf4 determines skeletal muscle identity in Myf5:Myod double-mutant mice. Nature 431, 466–471.
Kassar-Duchossoy, L., Giacone, E., Gayraud-Morel, B., Jory, A., Gomes, D., Tajbakhsh, S., 2005. Pax3/Pax7 mark a novel population of primitive myogenic cells during development. Genes Dev. 19, 1426–1431.
Kaufman, M.H., 1992. The Atlas of Mouse Development. Academic Press, Inc, San Diego, CA.
Kaul, A., Koster, M., Neuhaus, H., Braun, T., 2000. Myf-5 revisited: loss of early myotome formation does not lead to a rib phenotype in homozygous Myf-5 mutant mice. Cell 102, 17–19.
Kitzmann, M., Carnac, G., Vandromme, M., Primig, M., Lamb, N.J., Fernandez, A., 1998. The muscle regulatory factors MyoD and myf-5 undergo distinct cell cycle-specific expression in muscle cells. J. Cell Biol. 142, 1447–1459.
Lepper, C., Fan, C.M., 2010. Inducible lineage tracing of Pax7-descendant cells reveals embryonic origin of adult satellite cells. Genesis 48, 424–436.
Lepper, C., Partridge, T.A., Fan, C.M., 2011. An absolute requirement for Pax7-positive satellite cells in acute injury-induced skeletal muscle regeneration. Development 138, 3639–3646.
Lewandoski, M., 2001. Conditional control of gene expression in the mouse. Nat. Rev. Genet. 2, 743–755.
Ma, Q., Zhou, B., Pu, W.T., 2008. Reassessment of Isl1 and Nkx2-5 cardiac fate maps using a Gata4-based reporter of Cre activity. Dev. Biol. 323, 98–104.
McCarthy, J.J., Mula, J., Miyazaki, M., Erfani, R., Garrison, K., Farooqui, A.B., Srikuea, R., Lawson, B.A., Grimes, B., Keller, C., Van Zant, G., Campbell, K.S., Esser, K.A., Dupont-Versteegden, E.E., Peterson, C.A., 2011. Effective fiber hypertrophy in satellite cell-depleted skeletal muscle. Development 138, 3657–3666.
Miniou, P., Tiziano, D., Frugier, T., Roblot, N., Le Meur, M., Melki, J., 1999. Gene targeting restricted to mouse striated muscle lineage. Nucleic Acids Res. 27, e27.
Murphy, M.M., Lawson, J.A., Mathew, S.J., Hutcheson, D.A., Kardon, G., 2011. Satellite cells, connective tissue fibroblasts and their interactions are crucial for muscle regeneration. Development 138, 3625–3637.
Nagy, A., 2000. Cre recombinase: the universal reagent for genome tailoring. Genesis 26, 99–109.
Olguin, H.C., Yang, Z., Tapscott, S.J., Olwin, B.B., 2007. Reciprocal inhibition between Pax7 and muscle regulatory factors modulates myogenic cell fate determination. J. Cell Biol. 177, 769–779.
Ott, M.-O., Bober, E., Lyons, G., Arnold, H., Buckingham, M., 1991. Early expression of the myogenic regulatory gene, *myf-5*, in precursor cells of skeletal muscle in the mouse embryo. Development 111, 1097–1107.
Relaix, F., Rocancourt, D., Mansouri, A., Buckingham, M., 2004. Divergent functions of murine Pax3 and Pax7 in limb muscle development. Genes Dev. 18, 1088–1105.
Relaix, F., Rocancourt, D., Mansouri, A., Buckingham, M., 2005. A Pax3 /Pax7-dependent population of skeletal muscle progenitor cells. Nature 435, 948–953.
Rudnicki, M.A., Braun, T., Hinuma, S., Jaenisch, R., 1992. Inactivation of MyoD in mice leads to up-regulation of the myogenic HLH gene Myf-5 and results in apparently normal muscle development. Cell 71, 383–390.
Rudnicki, M.A., Schnegelsberg, P.N., Stead, R.H., Braun, T., Arnold, H.H., Jaenisch, R., 1993. MyoD or Myf-5 is required for the formation of skeletal muscle. Cell 75, 1351–1359.
Sambasivan, R., Comai, G., Roux, I.L., Gomes, D., Konge, J., Dumas, G., Cimper, C., Tajbakhsh, S., 2013. Embryonic founders of adult muscle stem cells are primed by the determination gene Mrf4. Dev. Biol. 381, 241–255.
Sassoon, D., Lyons, G., Wright, W.E., Lin, V., Lassar, A., Weintraub, H., Buckingham, M., 1989. Expression of two myogenic regulatory factors myogenin and MyoD1 during mouse embryogenesis. Nature 341, 303–307.

Sassoon, D.A., Garner, I., Buckingham, M., 1988. Transcripts of alpha-cardiac and alpha-skeletal actins are early markers for myogenesis in the mouse embryo. Development 104, 155–164.
Schienda, J., Engleka, K.A., Jun, S., Hansen, M.S., Epstein, J.A., Tabin, C.J., Kunkel, L.M., Kardon, G., 2006. Somitic origin of limb muscle satellite and side population cells. Proc. Nat. Acad. Sci. USA 103, 945–950.
Seale, P., Sabourin, L.A., Girgis-Gabardo, A., Mansouri, A., Gruss, P., Rudnicki, M.A., 2000. Pax7 is required for the specification of myogenic satellite cells. Cell 102, 777–786.
Smith, T.H., Kachinsky, A.M., Miller, J.B., 1994. Somite subdomains, muscle cell origins, and the four muscle regulatory factor proteins. J. Cell Biol. 127, 95–105.
Tajbakhsh, S., Borello, U., Vivarelli, E., Kelly, R., Papkoff, J., Duprez, D., Buckingham, M., Cossu, G., 1998. Differential activation of Myf5 and MyoD by different Wnts in explants of mouse paraxial mesoderm and the later activation of myogenesis in the absence of Myf5. Development 125, 4155–4162.
Tajbakhsh, S., Rocancourt, D., Cossu, G., Buckingham, M., 1997. Redefining the genetic hierarchies controlling skeletal myogenesis: Pax-3 and Myf-5 act upstream of MyoD. Cell 89, 127–138.
Thayer, M.J., Tapscott, S.J., Davis, R.L., Wright, W.E., Lassar, A.B., Weintraub, H., 1989. Positive autoregulation of the myogenic determination gene MyoD1. Cell 58, 241–248.
Wu, S., Wu, Y., Capecchi, M.R., 2006. Motoneurons and oligodendrocytes are sequentially generated from neural stem cells but do not appear to share common lineage-restricted progenitors in vivo. Development 133, 581–590.
Yamamoto, M., Shook, N.A., Kanisicak, O., Yamamoto, S., Wosczyna, M.N., Camp, J.R., Goldhamer, D.J., 2009. A multifunctional reporter mouse line for Cre- and FLP-dependent lineage analysis. Genesis 47, 107–114.
Yamamoto, M., Watt, C.D., Schmidt, R.J., Kuscuoglu, U., Miesfeld, R.L., Goldhamer, D. J., 2007. Cloning and characterization of a novel MyoD enhancer-binding factor. Mech. Dev. 124, 715–728.
Zammit, P.S., 2008. All muscle satellite cells are equal, but are some more equal than others? J. Cell Sci. 121, 2975–2982.